THE ASTROPHYSICAL JOURNAL, 482:L191–L194, 1997 June 20

MEASUREMENTS OF THE COSMIC-RAY POSITRON FRACTION FROM 1 TO 50 GeV

S. W. BARWICK,[1] J. J. BEATTY,[2] A. BHATTACHARYYA,[3] C. R. BOWER,[3] C. J. CHAPUT,[4] S. COUTU,[4] G. A. DE NOLFO,[2,5]
J. KNAPP,[6] D. M. LOWDER,[7] S. MCKEE,[4] D. MÜLLER,[8] J. A. MUSSER,[3] S. L. NUTTER,[9]
E. SCHNEIDER,[1] S. P. SWORDY,[8] G. TARLÉ,[4] A. D. TOMASCH,[4] AND E. TORBET[8]
(THE HEAT COLLABORATION)
Received 1997 February 6; accepted 1997 March 27

ABSTRACT

Two measurements of the cosmic-ray positron fraction as a function of energy have been made using the High-Energy Antimatter Telescope (HEAT) balloon-borne instrument. The first flight took place from Fort Sumner, New Mexico, in 1994 and yielded results above the geomagnetic cutoff energy of 4.5 GeV. The second flight, from Lynn Lake, Manitoba, in 1995, permitted measurements over a larger energy interval, from 1 to 50 GeV. We present results on the positron fraction based on data from the Lynn Lake flight and compare these with the previously published results from the Fort Sumner flight. The results confirm that the positron fraction does not increase with energy above ≈10 GeV, although a small excess above purely secondary production cannot be ruled out. At low energies the positron fraction is slightly larger than that reported from measurements made in the 1960s. This effect could possibly be a consequence of charge dependence in the level of solar modulation.
Subject headings: cosmic rays — elementary particles — instrumentation: detectors — ISM: abundances

1. INTRODUCTION

Cosmic-ray electrons and positrons interact with the interstellar medium exclusively through electromagnetic processes, such as synchrotron radiation and inverse Compton scattering, which do not significantly affect the nucleonic cosmic-ray components. For this reason, electrons are a unique probe of cosmic-ray confinement and source distribution in the Galaxy. The observed $e^{\pm}$ flux is dominated by negative electrons from primary acceleration sites. However, about 10% of the total flux is secondary particles, resulting from hadronic interactions between the nuclear cosmic rays and nuclei in the interstellar medium. These interactions produce electrons and positrons in roughly equal numbers. A number of observations (Agrinier et al. 1969; Buffington, Orth, & Smoot 1975; Müller & Tang 1987; Golden et al. 1987, 1994) indicate that the positron fraction, $e^+/(e^- + e^+)$, increases with energy at energies above 10 GeV. Such an increase would require either the appearance of a new source of positrons or a depletion of primary electrons. Confirming either of these possibilities would have a profound impact on our understanding of cosmic-ray sources. This motivated the construction of the HEAT (High-Energy Antimatter Telescope) instrument, which was designed to determine the positron fraction over a wide energy range, and with improved statistical and systematic accuracy. A first balloon flight (HEAT-94) was launched in 1994 from Fort Sumner, New Mexico, at a geomagnetic cutoff rigidity of roughly 4.5 GV. The results from this flight (Barwick et al. 1995) indicate that the positron fraction does not increase at high energies and that positrons may well be of entirely secondary origin. A subsequent publication (Golden et al. 1996) by another group has reported a positron fraction that is statistically consistent with both the HEAT result and the previous measurements.

In this Letter, we report the positron fraction measured during the second HEAT flight (HEAT-95). This flight was launched in 1995 from a location with a low cutoff rigidity (Lynn Lake, Manitoba), in order to permit measurements over a larger energy range of 1 GeV up to about 50 GeV. We present the results from this flight and compare this measurement with the previously reported data from HEAT-94. The two data sets have been analyzed in the same fashion, to avoid potential systematic differences in the final result.

2. DETECTOR

The HEAT detector is described in detail elsewhere (Barwick et al. 1997). It has a geometric acceptance of 473 cm^2 sr and consists of a magnetic spectrometer combined with a transition radiation detector (TRD), an electromagnetic calorimeter (EC), and time-of-flight (TOF) scintillators.

The magnetic spectrometer provides particle tracking through an array of drift tubes (DTs) in the magnetic field generated by a two-coil, warm-bore superconducting magnet. The DT array consists of 19 tracking layers in the bending plane and eight layers in the nonbending plane, each providing a single-point tracking resolution of ≈70 μm. The performance of the magnetic spectrometer as a whole can be characterized by the maximum detectable rigidity (MDR), which is the rigidity at which the momentum of the particle is equal to the error in the momentum measurement. The mean MDR achieved in both flights is 170 GV for electrons.

While the magnetic spectrometer determines the momen-

[1] Department of Physics and Astronomy, University of California at Irvine, Irvine, CA 92697-4575.
[2] Department of Physics and Department of Astronomy and Astrophysics, 104 Davey Laboratory, Pennsylvania State University, University Park, PA 16802.
[3] Department of Physics, Swain Hall West, Indiana University, Bloomington, IN 47405.
[4] Department of Physics, Randall Laboratory, 500 E. University Avenue, University of Michigan, Ann Arbor, MI 48109-1120.
[5] Department of Physics, Washington University, St. Louis, MO 63130.
[6] Institut für Experimentelle Kernphysik, Universität Karlsruhe, Postfach 3640, D-76021 Karlsruhe, Germany.
[7] Department of Physics, 366 LeConte Hall, University of California at Berkeley, Berkeley, CA 94720.
[8] Enrico Fermi Institute and Department of Physics, 933 E. 56th Street, University of Chicago, Chicago, IL 60637.
[9] Department of Physical Sciences, Eastern New Mexico University, Portales, NM 88130.

TABLE 1

SELECTION CRITERIA

Selection Description	HEAT-94 Selection Range	HEAT-95 Selection Range
TRD, DT track match	$\lvert \mathrm{int}_{DT} - \mathrm{int}_{TRD} \rvert < 25$ cm[a]	...
Charge = 1	$0.77e < Z < 1.5e$	$0.77e < Z < 1.5e$
Velocity = c	$0.5 < \beta < 2.0$	$0.8 < \beta < 2.0$
DT track χ^2	$\chi^2 < 10.0$	$\chi^2 < 10.0$
Track points	$n_{fit} > 9$	$n_{fit} > 8$
DTH rigidity error	$\mathrm{MDR}/\lvert R \rvert > 4$	$\mathrm{MDR}/\lvert R \rvert > 4$
TRD $e^{\pm}$ maximum likelihood	log ML > 2	log ML > 2
TRD chambers hit	$N_{TRD} = 6$	$N_{TRD} = 5$
TRD time slice	Neural net output > 0.5	Neural net output > 0.9
EC shower shape	$\chi^2_{EC} < 1.8$	$\chi^2_{EC} < 1.8$
EC shower start	$X_{start} < 0.8$ r.l.[b]	$X_{start} < 0.5$ r.l.[b]
Energy, momentum selection	$E > 3$ GeV, $\lvert p \rvert > 2.5$ GeV c^{-1}	$E > 1$ GeV, $\lvert p \rvert > 1$ GeV c^{-1}
$\lvert E/p \rvert$	$0.7 < \lvert E/p \rvert < 3.0$	$0.75 < \lvert E/p \rvert < 3.0$

[a] Where int_{DT} and int_{TRD} are the intercepts obtained in a fit of particle track in the DT and TRD systems.
[b] Radiation lengths.

tum and the sign of the particle's charge, additional measurements are needed to find the magnitude of the particle charge, the direction of particle traversal through the instrument, and the energy of electrons and positrons, and to reject hadronic background. The TRD provides electron identification and hadronic background rejection through the detection of transition X-rays, which can only be produced by particles possessing a large Lorentz factor ($\gamma > 10^3$). The TRD consists of six layers of proportional chambers and associated radiators. Using a maximum likelihood technique, we determine whether the signals induced on the TRD chamber cathodes indicate the presence of transition radiation or are consistent with ionization energy loss alone. In addition, the anode wires of each TRD chamber are read out in 25 ns time slices, in order to detect ionization clusters typical for X-ray signals. The time-slice data are analyzed with a neural-net technique and provide additional electron discrimination. The combination of maximum likelihood and time-slice analysis achieves a hadron rejection factor of $\geq$100 at an electron efficiency of 90%.

The EC consists of 10 layers of lead and plastic scintillators. The 10 EC signals recorded for an event are used to measure the primary energy of the particle, to determine the degree to which the longitudinal shower development matches that expected for an electron, and the depth at which the shower starts. These quantities are obtained from a covariance analysis, using accelerator calibrations of the EC and GEANT/FLUKA-based (Brun et al. 1994; Fassò et al. 1994) simulations. Over most of the energy range of interest, the energy resolution of the EC is 10%.

The event trigger included the requirement that the energy deposited in the last seven layers of the EC exceed that expected for a 0.5 GeV electron during the first flight, and a 1 GeV electron during the second flight. Although this requirement reduces the detection efficiency of electrons and positrons near the threshold energy, it does not affect the measured positron fraction, since the response of the EC to electrons and positrons of the same energy is identical. The hadron rejection factor for the trigger and EC is 200 at an electron efficiency of 90%. An additional energy-dependent hadron rejection factor of 1.5–10 is provided by a comparison between the energy measured in the calorimeter and the momentum measured by the spectrometer. The hadron rejection factors and electron efficiencies of the EC and TRD are determined from the flight data by using the particle identification obtained from one of the detectors to define clean samples of negative electrons and protons and then applying the electron selection criteria of the other detector to these samples.

The TOF system consists of a layer of four plastic scintillators at the top of the instrument and the first three scintillator layers of the EC. The top scintillators also provide a measurement of the magnitude of the particle charge to distinguish singly charged particles from heavier nuclei. The time-of-flight measurement is used to eliminate upward-going (albedo) particles, which mimic antiparticles in the spectrometer. The rejection power of the TOF system is sufficient to reduce the helium and albedo background to negligible levels.

3. FLIGHT SUMMARIES

The first HEAT flight, HEAT-94, took place from Fort Sumner, New Mexico, on 1994 May 3. The total time at float altitude was 29.5 hr, with a mean atmospheric overburden of 5.7 g cm^{-2}. During the flight, the geomagnetic cutoff rigidity at the detector varied between 4 and 4.5 GV. The second HEAT flight, HEAT-95, took place from Lynn Lake, Manitoba, on 1995 August 23. During this flight, the total time at float altitude was 26 hr. The mean atmospheric overburden was 4.8 g cm^{-2}, and the geomagnetic cutoff rigidity at the detector was well below 1 GV. The detector configuration was essentially the same for the two flights. In the HEAT-95 flight, one of the TRD chambers was inoperative as a result of a high-voltage system failure. The resulting loss of hadron rejection power is small and has been compensated for in the HEAT-95 analysis by slightly tighter electron selection criteria and correspondingly lower electron efficiency. All systems achieved comparable levels of performance in the two flights.

4. DATA ANALYSIS

Both data sets are subjected to essentially identical selection criteria to obtain a final sample of $e^{\pm}$. A complete list of these selections is shown in Table 1. The first set selects for singly charged, downward-going particles that have a well-determined momentum and a velocity measurement consistent with a $\beta = 1$ particle. The second set of criteria selects for $e^{\pm}$. The TRD maximum likelihood and time-slice analyses, in addition to the shower-shape analysis obtained from the EC, result in a

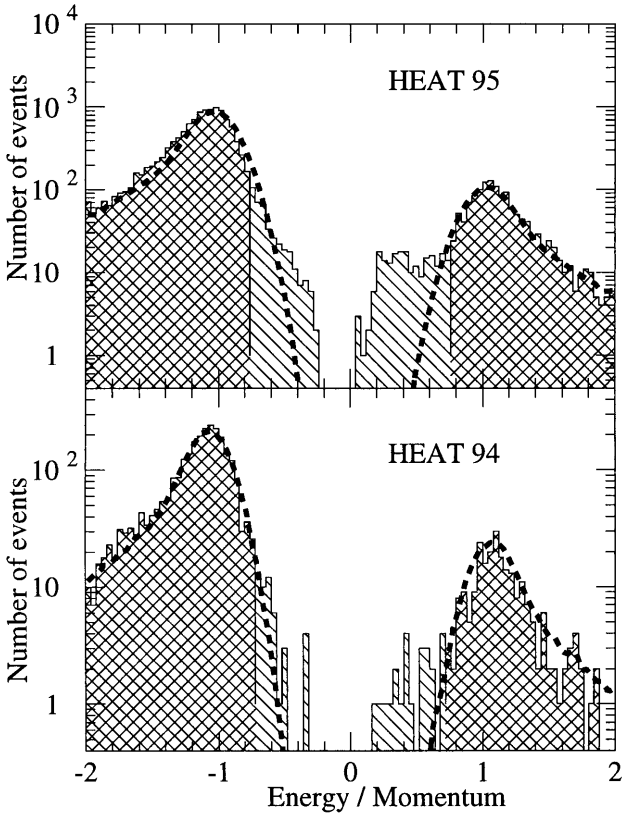

FIG. 1.—E/p distributions for $e^{\pm}$ selection. The dashed curve is a Monte Carlo calculation of the expected distributions. The crosshatched region indicates the E/p interval used in the final data sample. Note that the vertical scale is logarithmic.

clean sample of $e^{\pm}$. An energy and momentum selection appropriate to the geomagnetic rigidity cutoff of each flight is then made. Finally, we require that the energy, E, measured in the EC be consistent with the momentum, p, determined with the magnetic spectrometer. We evaluate the measured distributions of the ratio E/p in order to determine the residual background in the data sets. The E/p ratio should be unity for $e^{\pm}$ (subject to instrumental resolution) but will normally have a value less than unity for hadrons. The E/p distributions obtained for the two flights are shown in Figure 1. The E/p interval used in the final data sets is shown as the crosshatched region in this figure. The events falling outside this interval are primarily interacting hadrons that have survived the EC and TRD electron selections, along with electrons and positrons falling in the low-side tail of their E/p distribution. Applying the E/p selection symmetrically ensures that the positron fraction is not biased by this selection. The level of background in the positron sample is estimated by determining the shape of the E/p distribution for interacting hadrons, as well as that for electrons, and by fitting the measured E/p distribution for positron candidates to a superposition of these hadron and electron distributions for each E/p interval. This background represents $\approx 1\%$ of the positron counts at low energies, increasing to almost 10% at high energies.

Table 2 shows the corrected positron and electron counts and resulting positron fractions obtained from this analysis for the two data sets, binned according to the energy of the particle. The particle energy has been corrected for radiative losses to the top of the atmosphere. The corrected electron and positron counts shown in Table 2 were obtained by subtracting the hadronic background and the secondary positrons and electrons produced in the atmosphere from the raw counts. The atmospheric contribution was determined by a Monte Carlo simulation of hadronic interactions of cosmic rays in the atmosphere. Over most of the energy range of interest, the flux of positrons and electrons produced in the atmosphere is found to be $\approx 3\%$ of the total $e^{\pm}$ flux. An empirical estimate of the atmospheric contribution was also obtained from the flight data by comparing the positron fraction measured at depths less than 4 g cm^{-2} to that measured at depths greater than 6 g cm^{-2} as a function of energy. The atmospheric corrections to the positron fraction determined from the Monte Carlo simulation and from direct measurements agree within the statistical error of the direct measurement. The systematic error in the positron fraction resulting from uncertainties in the atmospheric background correction is estimated to be 1% for energies well above the geomagnetic cutoff.

5. RESULTS

The positron fraction as a function of energy is shown in Figure 2 for the two data sets, along with results from previous measurements by other groups, the predictions for purely secondary positron production (Protheroe 1982), and the predicted positron fraction based on recent work (Clem et al. 1996) that investigated the possible effect of charge sign–dependent modulation. The HEAT-94 data points shown in Figure 2 are essentially those previously published (Barwick et al. 1995). Minor changes, resulting from a refinement of the

TABLE 2

RESULTS

Energy (GeV)	$E_{\rm mean}$ (GeV)	$n_{e^+}^{94}$	$n_{e^-}^{94}$	$n_{e^+}^{95}$	$n_{e^-}^{95}$	f^{94} [a]	f^{95}	$f^{\rm comb.}$
1.0–1.5	1.36	...	...	65.9	475.3	...	0.122 ± 0.016	0.122 ± 0.016
1.5–2.0	1.76	...	...	236.3	1780.2	...	0.117 ± 0.008	0.117 ± 0.008
2.0–3.0	2.46	...	...	342.6	3300.6	...	0.094 ± 0.005	0.094 ± 0.005
3.0–4.5	3.64	...	...	205.5	2631.6	...	0.072 ± 0.005	0.072 ± 0.005
4.5–6.0	5.14	48.6	730.5	62.6	1218.6	0.062 ± 0.010	0.049 ± 0.006	0.054 ± 0.006
6.0–8.9	7.20	90.1	1049.3	48.8	846.5	0.079 ± 0.008	0.055 ± 0.008	0.068 ± 0.006
8.9–14.8	11.0	38.6	571.9	20.0	455.6	0.063 ± 0.010	0.060 ± 0.012	0.062 ± 0.008
14.8–26.5	18.4	13.7	227.8	6.9	148.1	$0.057^{+0.019}_{-0.014}$	$0.044^{+0.025}_{-0.016}$	0.052 ± 0.013
26.5–50.0	32.3	2.1	41.2	2.1	29.4	$0.048^{+0.059}_{-0.027}$	$0.070^{+0.081}_{-0.045}$	$0.057^{+0.042}_{-0.027}$

[a] Where $f = e^+/(e^- + e^+)$.

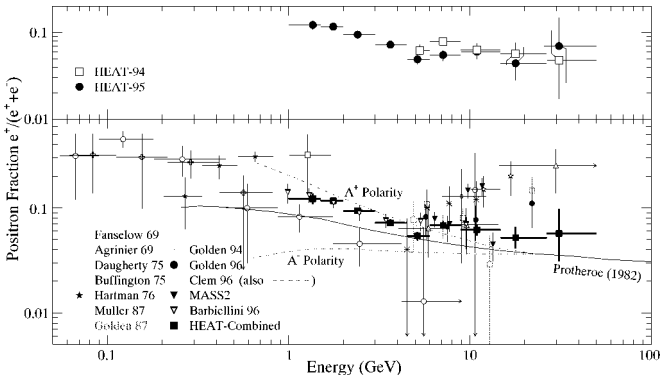

FIG. 2.—Positron fraction as a function of energy obtained from the two data sets. The error bars applied to the HEAT data points represent statistical errors only. The curve labeled "Protheroe (1982)" is calculated for a purely secondary positron origin, assuming the leaky-box approximation for Galactic propagation. Points for MASS2 are from Hof et al. (1995).

atmospheric secondary correction, include the elimination of events with energies between 4.5 and 5 GeV, for which the secondary correction is more uncertain as a result of the proximity of the geomagnetic cutoff. The HEAT-95 measurement reinforces the conclusion that the positron fraction does not increase in the 10–50 GeV energy range: the results of the two measurements are consistent with each other and with a general decrease of the positron fraction with energy. Both data sets do indicate an overabundance of positrons compared with the prediction of Protheroe (1982) at all energies, but this disagreement may not be taken too seriously, as the model itself has inherent uncertainties. For example, the predicted positron fraction scales with the ratio of the absolute proton to electron flux, and the uncertainties in these quantities are directly reflected in the positron fraction. The combined data set suggests the presence of a feature in the positron fraction in the energy range from 7 to 20 GeV. Positron production mechanisms have been suggested (e.g., Kamionkowski & Turner 1991) that would lead to an excess of positrons in this energy region, but the uncertainties in our data do not permit a definite conclusion, and further measurements are required to confirm that this feature exists.

At energies below a few GeV, our measured positron fraction is significantly higher than that reported in 1969 by Fanselow et al., while it is in excellent agreement with a recent measurement by an independent group (Barbiellini et al. 1996). As the earlier measurement was performed at a different period in the solar activity cycle, it may be tempting to interpret the results as being affected by the charge dependence in the solar modulation. This effect, and its impact on the positron fraction measured at Earth, has been investigated by several groups (Moraal, Jokipii, & Mewaldt 1991; Clem et al. 1996). Clem et al. have developed a model based on the observed systematic difference in the correlation between the electron flux measured in space by the *International Cometary Explorer* instrument and ground-based neutron monitor measurements for the 1980 and 1990 solar polarity epochs. This model predicts that the present solar epoch favors the transmission of positive charge species, resulting in an enhancement in the measured positron fraction over the Galactic value. While our observations may lend some support to the hypothesis of charge sign–dependent solar modulation, a definitive test of this hypothesis will have to wait until the onset of the next solar epoch, about the year 2000.

We gratefully acknowledge assistance from D. Bonasera, E. Drag, D. Ellithorpe, M. Gebhard, W. Johnson, D. Kouba, R. Northrup, and J. Robbins. We also thank the National Scientific Balloon Facility balloon crews for their excellent support of the HEAT flights. This work was supported by NASA grants NAG 5-5059, NAG 5-5069, NAG 5-5070, NAGW-5058, NAGW-1995, NAGW-2000, and NAGW-4737 and by financial assistance from our universities.

REFERENCES

Agrinier, B., et al. 1969, Lett. Nuovo Cimento, 1, 53
Barbiellini, G., et al. 1996, A&A, 309, L15
Barwick, S. W., et al. 1995, Phys. Rev. Lett., 75, 360
———. 1997, Nucl. Instrum. Methods Phys. Res., submitted
Buffington, A., Orth, C. D., & Smoot, G. F. 1975, ApJ, 199, 669
Clem, J. M., Clements, D. P., Esposito, J., Evenson, P., Huber, D., L'Heureux, J., Meyer, P., & Constantin, C. 1996, ApJ, 464, 507
Daugherty, J. K., Hartman, R. C., & Schmidt, P. J. 1975, ApJ, 198, 493
Fanselow, J. L., Hartman, R. C., Hildebrand, R. H., & Meyer, P. 1969, ApJ, 158, 771
Fassò, A., Ferrari, A., Ranft, J., & Sala, P. R. 1993, in Proc. 4th Int. Conf. on Calorimetry in High Energy Physics, ed. A. Menzione & A. Scribano (Singapore: World Sci.), 493
Giani, S., et al. 1994, GEANT: Detector Description and Simulation Tool (CERN Program Libr. Long Write-up W5013) (version 3.21; Geneva: CERN)
Golden, R. L., et al. 1994, ApJ, 436, 769
Golden, R. L., Mauger, B. G., Horan, S., Stephens, S. A., Daniel, R. R., Badhwar, G. D., Lacy, J. L., & Zipse, J. E. 1987, A&A, 188, 145
Golden, R. L., et al. 1996, ApJ, 457, L103
Hartman, R. C., & Pellerin, C. J. 1976, ApJ, 204, 927
Hof, M., et al. 1995, Proc. 24th Int. Cosmic-Ray Conf. (Rome), 3, 1
Kamionkowski, M., & Turner, M. S. 1991, Phys. Rev. D, 43, 1774
Moraal, H., Jokipii, J. R., & Mewaldt, R. A. 1991, ApJ, 367, 191
Müller, D., & Tang, K. 1987, ApJ, 312, 183
Protheroe, R. J. 1982, ApJ, 254, 391